Research Article

Received: 8 December 2020 Revised: 8 February 2021 Accepted article published: 15 March 2021 Published online in Wiley Online Library:

(wileyonlinelibrary.com) DOI 10.1002/jsfa.11224

A magnetic relaxation switch sensor for determination of 17β-estradiol in milk and eggs based on aptamer-functionalized Fe_3O_4@Au nanoparticles

Xin Wang,[a*] Kaili Pei,[a] Hanying Sun[a,b] and Qi Wang[a]

Abstract

BACKGROUND: A simple and rapid detection method for 17β-estradiol (E_2) in complex food matrix is greatly desirable. A magnetic relaxation switch (MRS) sensor for detecting E_2 based on the aptamer-functionalized gold-coated iron oxide (Fe_3O_4@Au) nanocomposite was designed in this study. Fe_3O_4@Au nanoparticles (NPs) played as a 'switch' between dispersed and aggregated states, while aptamer served as the recognition unit.

RESULTS: According to the sensing effect of monocomponent relaxation time (T_{2W}) for E_2, the volume ratio of aptamers to Fe_3O_4@Au, the sodium chloride (NaCl) concentration, the concentration of Fe_3O_4@Au@Apt, and reaction time were optimized to be 4:1, 0.03 mol L^{-1}, 4 μmol L^{-1} and 15 min, respectively. For the analysis of food sample, the E_2 was quantified over a concentration range of 1 to 100 nmol L^{-1} with a detection limit of 7.6 nmol L^{-1} for milk samples, while a linearity range of 20 to 100 nmol L^{-1} and a detection limit of 8.57 nmol L^{-1} for egg samples.

CONCLUSION: These results exhibited that the MRS sensor could be a promising platform for the rapid detecting of E_2 in food sample.

Supporting information may be found in the online version of this article.

Keywords: biosensor; magnetic relaxation switch sensor; 17β-estradiol; Fe_3O_4@Au nanocomposites; aptamer

INTRODUCTION

As a natural environmental estrogen, 17β-estradiol (E_2) can cause adverse health effects,[1] particularly leading to an increased incidence of male reproductive disorders and tumor.[2,3] Considering that E_2 can be easily absorbed via the food chain, humans may be greatly affected due to bioaccumulation even at low concentration of E_2.[4] Recently, E_2 has been detected in animal-derived food, such as pork, chicken,[5] grass carp,[6] eggs,[7] milk[8] and other dairy products.[9] Therefore, it has become necessary to develop a sensitive and reliable detection method for the determination of trace E_2 residues in complex food matrixes.

Up to now, several analytical techniques, such as high-performance liquid chromatography (HPLC),[10,11] gas chromatography–mass spectrometry (GC–MS),[12–14] and liquid chromatography–mass spectrometry (LC–MS),[15,16] have been successfully employed for E_2 detection. Although these methods possess high selectivity and sensitivity, it is undeniable that they require expensive equipment, skilled operators, complicated pretreatment, usage of harmful solvents, and time-consuming process.[4] Hence, to meet the high demand of rapid, real-time, and on-site measurement, a rapid and sensitive detection method for E_2 determination is still in need for further research.

Besides the biosensor-based techniques based on colorimetric,[17,18] fluorogenic,[19–21] and electrochemical properties,[22] the magnetic relaxation switch (MRS) sensor has attracted increasing attention. In MRS detection, the presence of a target substance will change the dispersed and aggregated states of nanoparticles (NPs), resulting in the change of the spin–spin relaxation time (T_2) of surrounding water protons.[23] Then, the relationship between the change of T_2 ($\triangle T_2$) and the target substance can be used to quantify the target in the samples. Because the MRS sensor only relies on magnetic signals, it is useful for the detection of target substances in turbid and light-impermeable systems. Up to now, the MRS sensors have been developed to identify and quantify a large variety of targets, such as metal ions,[24–26] protein,[27] nucleic acid,[28] enzyme activity,[29] bacteria,[30,31] virus[32] and small molecules,[33,34] etc. Meanwhile, compared with the monocomponent material, composite NPs of gold-coated iron oxide (Fe_3O_4@Au) is a new type of composite NP with stronger optical, magnetic and catalytic properties and thermal stability.[35]

* Correspondence to: X Wang, School of Medical Instrument and Food Engineering, University of Shanghai for Science and Technology, Shanghai 200093, China. E-mail: 18918629281@126.com

a School of Medical Instrument and Food Engineering, University of Shanghai for Science and Technology, Shanghai, China

b Graduate School of Fisheries and Environmental Sciences, Nagasaki University, Nagasaki, Japan

Biosensors based on Fe_3O_4@Au have been designed and applied to analyze mercury (Hg),[2–24], thrombin[29] and catechol.[36] However, to our knowledge, the determination of E_2 by magnetic relaxation properties of Fe_3O_4@Au has not been reported.

However, aptamers, which can bind with target molecules with high affinity and specificity, has been preferred in analytical biosensor as recognition elements.[17] Based on the E_2-specific aptamer,[37] colorimetric,[38] fluorescent,[21] electrochemical[39] biosensors have been designed. These researches provided helpful approaches for the rapid and sensitive detection of E_2.

Therefore, in this article, we designed an aptamer-based Fe_3O_4@Au sensing platform by combining the MRS technique and the aptamer together for detecting E_2 in complex food sample. The detection conditions were optimized and the performance of the method was evaluated. Then, milk and eggs were chosen to evaluate the feasibility of this sensor for practical application. This research could prove the feasibility of using the proposed MRS sensor as a high sensitivity and selectivity method for the rapid detection of E_2 in food samples.

EXPERIMENTAL

Reagents

The E_2 (98%), bisphenol A (BPA, > 99%), methyltestosterone (MT, 98%), diethylstilbestrol (DES, 99%), progesterone (P_4, 99%), chloroauric acid ($HAuCl_4$, 48–50%), citric acid (99.5%), sodium citrate dihydrate (99%) and methanol (99.8%) were purchased from Macklin Chemical Reagent Co., Ltd (Shanghai, China). E_2 aptamers (5′-GCTTCCAGCTTATTGAATTACACGCAGAGGGTAGCGGCTCTGCGCA TTCAATTGCTGCGCGCTGAAGCGCGGAAGC-3′)[37] were synthesized and purified by Sango Corp. (Shanghai, China). The dissociation constant of the E_2-aptamer was 0.13 μmol L^{-1} . Iron(II) sulfate tetrahydrate ($FeSO_4{\cdot}4H_2O$), iron(III) chloride hexahydrate ($FeCl_3{\cdot}6H_2O$), sodium hydroxide (NaOH), and ammonia ($NH_3{\cdot}H_2O$) were purchased from Sinopharm Chemical Reagent Co. Ltd (Shanghai, China). The earlier mentioned reagents were of analytical grade and used as received. Milk and eggs were purchased from a supermarket in Shanghai, China.

Instrumentation and characterization

The value of T_2 was measured by a low-field pulsed nuclear magnetic resonance (NMR) analyzer (miniPQ001, Suzhou Niumag Analytical Instrument Corporation, Suzhou, China). The strength of the magnetic field was 0.467 T and the spectrometer frequency (SF) was 20 MHz. The ultraviolet-visible (UV-vis) absorption spectra of NPs were obtained by using a Synergy H4 multi-mode microplate reader (BioTek Instrumrnts, Winooski, VT, USA). The hydrodynamic diameter and polydispersity index (PDI) of NPs were measured by dynamic light scattering (DLS) with a NanoBrook 173plus (Brookhaven Instruments Corporation, Austin, TX, USA). The morphology of NPs was observed using transmission electron microscopy (TEM; JEOL2100F, JEOL, Tokyo, Japan) by placing a drop of sample solution on a transmission electron microscope copper grid. The concentration of NPs was obtained using inductively coupled plasma atomic emission spectroscopy (ICP-AES; Agilent Technologies Inc., Beijing, China). The magnetic properties of NPs were evaluated by the transverse relaxivity (r_2), which was calculated from the slope of $1/T_2$ relaxation rate as a function of the iron (Fe) concentration graph.[40]

Optimization of incubation conditions of Fe_3O_4@Au and aptamer

For better detection effect, the volume ratio of aptamers and Fe_3O_4@Au NPs were optimized from 0.5:1, 1:1, 2:1, 3:1, 4:1, 5:1 and 6:1 according to their absorbance spectra. Under the same volume ratio of aptamers and Fe_3O_4@Au NPs (4:1), we optimized the incubation time from 0.5 to 4 h. Finally, the sodium chloride (NaCl) concentration was optimized from 0.02, 0.03, 0.04, 0.05 and 0.06 mol L^{-1} .

Procedure of MRS sensor

A certain volume of Fe_3O_4@Au@Apt dispersion, NaCl (0.3 mol L^{-1}) and deionized water were added to the chromatographic bottle, respectively. The resulting mixture was dispersed by ultrasound for 30 s and then heated in a 35 °C water bath for 5 min. Subsequently, the sample of 150 μL E_2 with different concentrations (1000, 100, 10, 1 and 0.1 nmol L^{-1}) was added and reacted at 35 °C for a certain period, then the chromatographic bottle was transferred into a 15 mm low-field nuclear magnetic resonance (LF-NMR) tube. The temperature of the magnet is 35.0 °C. The Carr–Purcell–Meiboom–Gill (CPMG) pulse sequence[41] was used to study the spin–spin relaxation. The related parameters were as follows: spectral bandwidth (SW) = 125 kHz, SF = 20 MHz, regulate analog gain 1 (RG1) = 20.0 db, regulate digital gain 1 (DRG1) = 3, pre-amp regulate gain (PRG) = 1, recycle time (TW) = 3000 ms, number of scan (NS) = 4, echo time (TE) = 0.5 ms. Then the MultiExp Inv Analysis software (Suzhou Niumag Analytical Instrument Corporation), a modified algorithm of simultaneous iterative reconstruction technique (SIRT), was used to invert the exponentially decaying signals into mono-exponential distribution, from which we can get the monocomponent relaxation time (T_{2w}), a variable that reflects the overall relaxation distribution of the sample. The change of T_{2w} (ΔT_{2w}) was calculated using the following equation:

$$\Delta T_{2w} = T'_{2w} - T_{2w} \quad (1)$$

where the T'_{2w} was the relaxation time of test solution with different concentrations of E_2 and the T_{2w} was the relaxation time of Fe_3O_4@Au@Apt solution without E_2.

Optimization of the detecting condition

To determine the optimized dilution ratio (the optimized concentration) of the Fe_3O_4@Au@Apt, dilution ratios (concentration) of the Fe_3O_4@Au@Apt were set as 100, 200, 300, 400 and 500 times (12, 6, 4, 3 and 2.4 μmol L^{-1}), while the reaction time was 15 min. Under the optimized concentration of the Fe_3O_4@Au@Apt, the reaction time was set as 5, 10, 15, 20 and 25 min to find optimum reaction time.

Evaluation of sensitivity and specificity of detection method

In order to evaluate the sensitivity of the detection method, different concentrations of E_2 (1, 5, 10, 50 and 100 nmol L^{-1}) were added to the optimized system for detection. The working curve was drawn according to the change of T_{2w} and the limit of detection (LOD) was calculated using the following equation.[25]

$$\mathrm{LOD} = KS_b/S \quad (2)$$

where S_b is the standard deviation of the blank measures (repeating 11 times), $K = 3$ and S is the sensitivity of the method.

MT, DES, BPA and P_4, whose structures are similar to E_2, were used to evaluate the specificity of the detection method. The E_2 analogs, at a concentration of 50 nmol L^{-1}, were added to the optimized system for detection. The system without E_2 and analogs was used as a control group.

Detection of E_2 in spiked samples

Milk and eggs were used to validate the feasibility of the method, and the samples were pre-treated according to the methods of Li *et al.*[42] and Zou *et al.*[30] with minor modification. Milk and eggs were spiked with E_2 at different concentrations (the concentrations of E_2 in the milk system and the eggs system were 1–100 nmol L^{-1} and 20–100 nmol L^{-1}, respectively). Afterward, 2 mL trichloroacetic acid (10%) and 2 mL trichloromethane were added to the beaker with 4 mL sample. After oscillating for 1 min, the mixture was dispersed by ultrasound for 15 min, thereafter was centrifuged (13 000 rpm) for 3 min. The supernatant was centrifuged at 10000 rpm for 3 min and the resulting supernatant was detected by the earlier method.

To calculate the recovery concentration, relative standard deviation (RSD) and recovery rate, the concentrations of E_2 in the milk system were set as 10, 50, and 100 nmol L^{-1}, and the concentrations of E_2 in the eggs system were set as 20, 60, and 100 nmol L^{-1}, respectively. Each point was analyzed five times.

Statistical analysis

All the tests were performed in triplicate except for special instructions and $P < 0.05$ was considered statistically significant. Origin 8 (OriginLab Corporation, Northampton, UK) was used to draw the figures. SPSS 17 (SPSS Inc., Chicago, IL, USA) was used to perform Statistical analysis and the different influencing factors on A650/A530 were analyzed by analysis of variance (ANOVA).

RESULTS AND DISCUSSION

Mechanism of detection

A schematic of the designed MRS assay based on the aptamer-functionalized Fe_3O_4@Au NPs is shown in Scheme 1.

Generally, the Fe_3O_4@Au NPs were well dispersed due to electrostatic stabilization with negative charge of citrate. When NaCl was added, the negative charges on the surface of Fe_3O_4@Au would be screened by the added cations, resulting in the aggregation of NPs. However, when the nucleic acid aptamers adsorbed on the surface of Fe_3O_4@Au by electrostatic interaction, the long-ranged electrostatic repulsion of aptamers can enhance the stability of Fe_3O_4@Au NPs against salt-induced aggregation, and thus Fe_3O_4@Au@Apt particles remained stable under a certain salt concentration.[43] In the presence of target, aptamer would bind with target and detach from the surface of Fe_3O_4@Au because of higher affinities between aptamer and target. Then less protection of aptamers may result in the aggregation of Fe_3O_4@Au induced by salt. The dispersed and aggregated states of Fe_3O_4@Au NPs would lead to the formation of a local non-uniform magnetic field, and this change can affect the spin–spin relaxation behavior of surrounding water protons. Since the change of T_{2w} ($\triangle T_{2w}$) is dependent on the amounts of target substance (E_2), this relationship can be used to quantify the target in the samples by establishing a standard curve.

Preparation and characterization of Fe_3O_4@Au

As shown in Supporting Information, Fig. S1(a), due to the heavy atom effect,[44] the color of Fe_3O_4@Au were darker than the uncoated Fe_3O_4 NPs, which were the faint and tiny particles on the background.[45] The obtained Fe_3O_4@Au NPs showed a core-shell structure and the excellent dispersibility with an averaged diameter of 20 nm. However, due to the hydrodynamic shell,[46] the average hydrodynamic diameter of Fe_3O_4@Au obtained by DLS was much higher than TEM, that is, 260.65 nm, shown in Fig. S1(b), and the PDI of 0.21 also indicated that the Fe_3O_4@Au particle was relatively uniform. A similar result was reported by Banerjee *et al.*,[47] where a core-shell Fe_3O_4@Au with a size of 14.31 (± 3.01) nm was obtained and used as optical probe for arsenic(III). Moreover, the ICP-AES analysis of Fe_3O_4@Au NPs showed that the concentrations of Fe and Au ions were 6 and 1.2 mmol L^{-1}, respectively.

The UV-vis spectrum of Fe_3O_4@Au in Fig. S1(c) showed a characteristic absorption peak of AuNPs at about 530 nm. Compared with AuNPs, Fe_3O_4@Au had a wider UV-vis absorption band, indicating that the Au shell had been successfully coated on the Fe_3O_4 surface.[48] This was in good agreement with the TEM result. As shown in Fig. S1(d), the r_2 value of Fe_3O_4@Au NPs was 89.173 mmol L^{-1} s^{-1}, while Liang *et al.*[29] also prepared a core-shell Fe_3O_4@Au NPs with a smaller r_2 value of 20.46 mmol L^{-1-} s^{-1}. A higher r_2 value would be helpful for improving the sensitivity of MRS assay,[49] therefore, the prepared Fe_3O_4@Au NPs are suitable for use as a MRS probe.

Optimization of incubation conditions of Fe_3O_4@Au and aptamer

The concentration of aptamer

The concentration of aptamers is one of the key factors for the construction of MRS sensor. As shown in Fig. 1(A), the UV-vis spectra of reaction systems before and after incubation showed characteristic absorption peaks of aptamer at 260–290 nm, and the absorption peaks of the supernatant after incubation were relatively decreased. When the volume ratio of aptamer to Fe_3O_4@Au was 4:1, the A_{260} of the reaction system before incubation was 2.45, while the A_{260} of the supernatant after incubation was significantly reduced to 0.89, indicating that the aptamers in the system had been successfully adsorbed on the surface of Fe_3O_4@Au.[50]

According to the method of Liang *et al.*,[29] the amount of aptamer immobilized on the Fe_3O_4@Au was obtained by subtracting the A_{260} of the supernatant containing the free aptamer from that of the original aptamer, that is, ΔA_{260}. The amount of nucleic acid aptamers bound to NPs can be reflected by ΔA_{260}. As the ratio of E_2apt to Fe_3O_4@Au increased from 0.5: 1 to 4: 1, shown in Fig. 1(B), the ΔA_{260} of the system increased from 0.12 to 1.56, demonstrating that aptamers adsorbed on the Fe_3O_4@Au surface. And when the ratio of E_2apt to Fe_3O_4@Au increased to 5:1, the ΔA_{260} increased to 1.6. However, no significant change of ΔA_{260} was observed when the ratio of E_2apt to Fe_3O_4@Au increased to 6:1, indicating that the number of aptamers adsorbed on Fe_3O_4@Au surface had almost reached saturation. In general, when the E_2apt to Fe_3O_4@Au ratio was between 4:1–5:1, sufficient aptamers can be adsorbed on the surface of Fe_3O_4@Au, which is beneficial for the target recognition and detection.

Meanwhile, the change of A_{650}/A_{530} of the system was used to reflect the aggregation of Fe_3O_4@Au caused by the addition of aptamers. As shown in Fig. 1(C), when the volume ratio of E_2apt to Fe_3O_4@Au increased from 0.5: 1 to 4: 1, the A_{650}/A_{530} slightly increased from 0.9 to 0.933, indicating that Fe_3O_4@Au@Apt still presented a good dispersion state. However, with the ratio of E_2apt to Fe_3O_4@Au increased to 5:1, the A_{650}/A_{530} significantly increased to 0.982, indicating that the Fe_3O_4@Au@Apt became

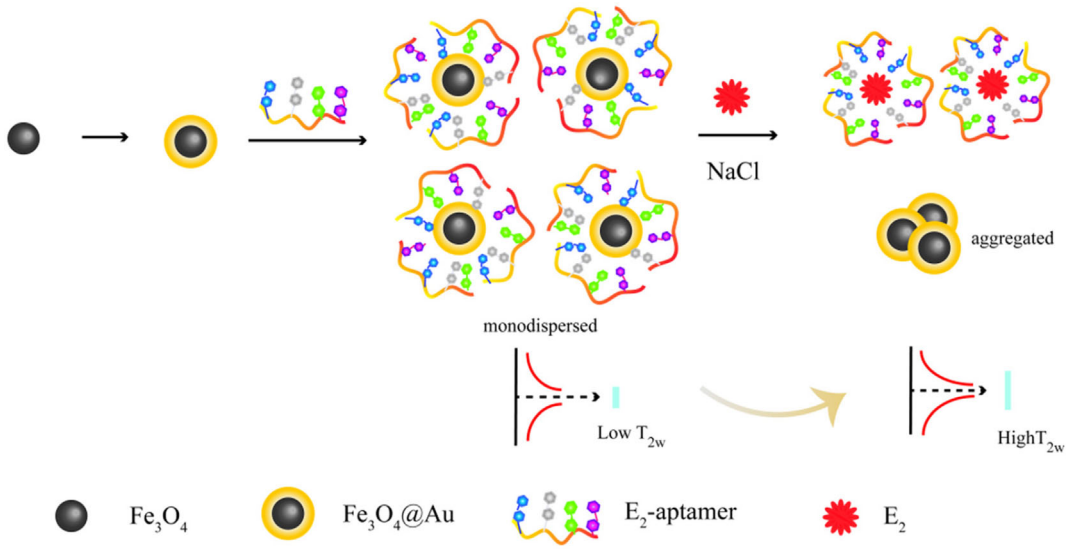

Scheme 1. Schematic representation of the magnetic relaxation switch sensor for rapid determination of 17β-estradiol based on aptamer-functionalized Fe_3O_4@Au nanoparticles.

aggregated, which was not expected for the subsequent analysis. Therefore, 4:1 was selected as the optimal volume ratio of E_2apt to Fe_3O_4@Au. However, this result was different from that reported by Kim *et al.*,[51] who designed a colorimetric aptasensor for the detecting of oxytetracycline (OTC), and the molar ratio of aptamer to Au NPs was chosen as 50:1, far greater than our molar ratio of 3:1. This may be explained by the fact that the interaction between aptamer and NPs was influenced by the structure of aptamer,[52,53] and the aptamers of E_2 and OTC possess different structures.[51,54]

The incubation time of Fe_3O_4@Au and aptamer

The adsorption of aptamers onto the Fe_3O_4@Au was also affected by the incubation time. As shown in Fig. 1(D), after a period of incubation, all the A_{260} values of the system became lower. When incubated for 2 h, the A_{260} value of the supernatant was the lowest, only 0.893. Furthermore, Fig. 1(E) showed that the ΔA_{260} value increased during the 0.5 to 2 h incubation, and reached the maximum value (1.558) at 2 h, indicating that the adsorption between aptamers and Fe_3O_4@Au was completed. However, the changes of A_{650}/A_{530}, shown in Fig. 1(F), was not significant, indicating that incubation time had little effect on the aggregation of Fe_3O_4@Au. Therefore, the incubation time for Fe_3O_4@Au and the aptamer was determined as 2 h, to ensure the adsorption of aptamers onto Fe_3O_4@Au.

The concentration of NaCl

The NaCl concentration is closely related to the stability, sensitivity, and reproducibility of the method. However, too high a concentration of NaCl is likely to lead to the aggregation of Fe_3O_4@Au@Apt,[55] which would affect the detection results. Figure 1(G) shows that the A_{650}/A_{530} of Fe_3O_4@Au@Apt showed a slight upward trend with the increase of NaCl concentration during incubation, however, the change was still not significant compared with the control group (0.935) even incubated for 25 min, when the NaCl concentration was no more than 0.03 mol L^{-1}, showing that the NPs dispersed well. While the A_{650}/A_{530} of the system with 0.04 mol L^{-1} NaCl significantly increase to 0.971, indicating the aggregation of NPs. Therefore, to avoid the salt-induced aggregation of Fe_3O_4@Au@Apt, the concentration of NaCl was selected as 0.03 mol L^{-1}, and the reaction time was controlled within 25 min in the subsequent experiments. Similar results were reported by Li *et al.*[56] and Ma *et al.*,[43] who employed aptamer-functional Au NPs as a colorimetric sensor to detect microcystin-LR and tobramycin, in which 0.024 and 0.04 mol L^{-1} were chosen as the optimal concentrations of NaCl to induce Au NP aggregation.

Optimization of the detection system

The concentration of Fe_3O_4@Au@Apt

The concentration of the magnetic nanoparticle (MNPs) needs to be optimized according to the concentration of the target.[57] Only when the concentration of the MNPs and the target reaches the appropriate ratio, the change of the T_2 is significant, which is more conducive to improving the detection sensitivity. The changes of T_{2w} and ΔT_{2w} of the system at different concentrations of Fe_3O_4@Au@Apt and E_2 are shown in Fig. 2(A,B). As shown in Fig. 2(A), at a fixed target concentration, the T_{2w} relatively decreased with the increase of Fe_3O_4@Au@Apt concentration. When the concentration of Fe_3O_4@Au@Apt increased from 2.4 to 12 μmol L^{-1}, the T_{2w} value of the blank group decreased from 1062.68 to 308.37 ms, and the T_{2w} value of the system with 1 nmol L^{-1} E_2 decreased from 1306.61 to 396.38 ms. These phenomena were due to the fact that the evenly presented magnetic NPs could induce the local magnetic field inhomogeneities.[58,59] These inhomogeneities dephase the precessions of the surrounding water proton spins and generated a reduction of the T_{2w} of water.[60] However, when the concentration of MNPs was low, the inhomogeneities became weaker and the T_{2w} value would relatively increase. When the solution was overdiluted, the effect of MNPs on the system was negligible, and T_{2w} of the system was close to that of water.

However, at a fixed Fe_3O_4@Au@Apt concentration, the T_{2w} value of the blank group was lower than that of the experimental group, and the T_{2w} increased with the increase of E_2 concentration. When the concentration of Fe_3O_4@Au@Apt was 4 μmol L^{-1}, the T_{2w} of the blank group was 722.34 ms, while the T_{2w} of the systems with 0.1 and 1000 nmol L^{-1} E_2 were respectively increased to

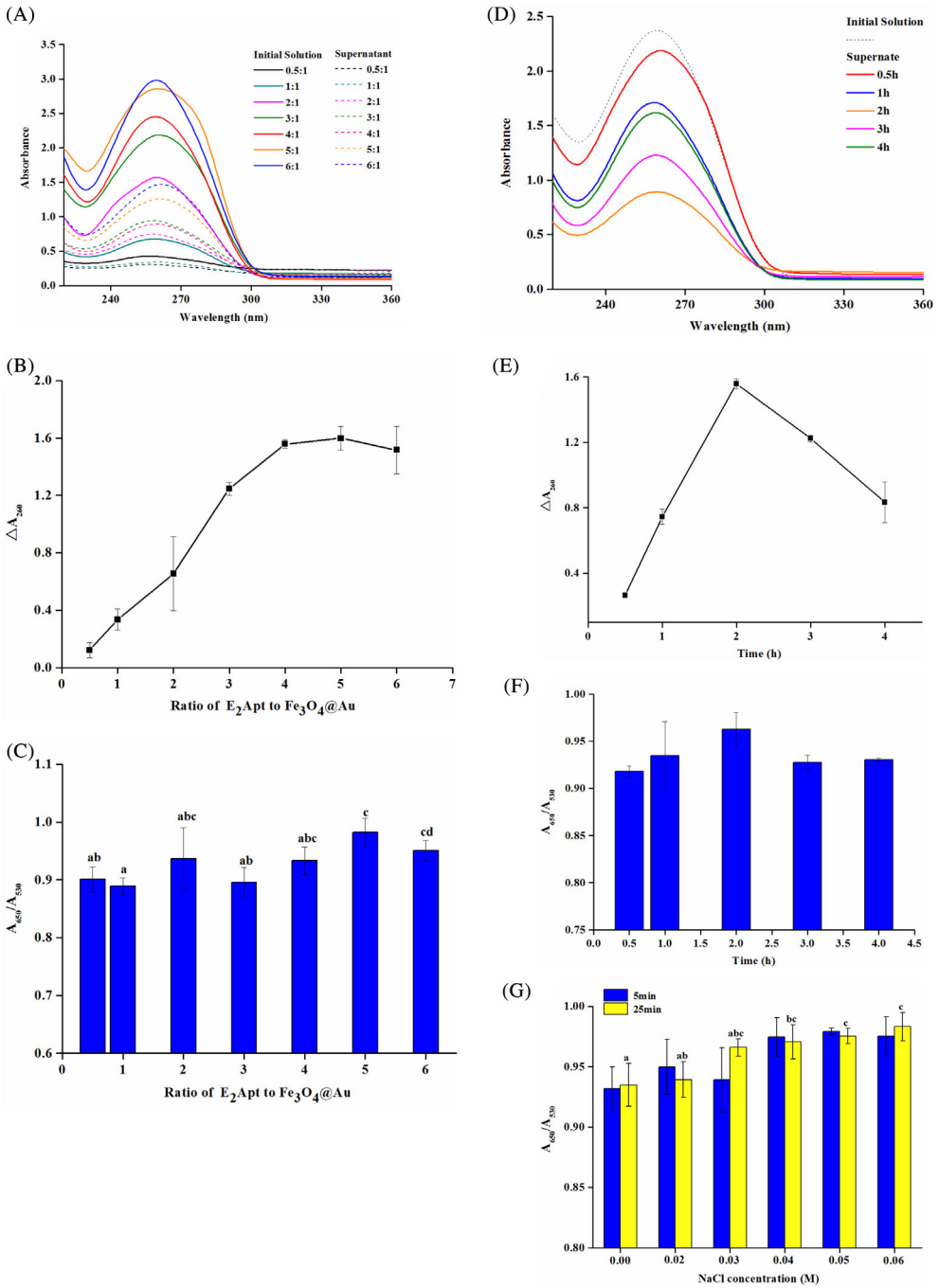

Figure 1. Optimization of incubation conditions for Fe_3O_4@Au and E_2apt. (A) UV-vis absorption spectra of system before and after incubation with different ratios of E_2apt to Fe_3O_4@Au. (B) The ΔA_{260} of the system with different ratio of E_2apt to Fe_3O_4@Au. (C) The A_{650}/A_{530} of the system under different ratio of E_2apt to Fe_3O_4@Au. (D) UV-vis absorption spectra of E_2apt and Fe_3O_4@Au system at different incubation time. (E) The ΔA_{260} of E_2apt and Fe_3O_4@Au system at different incubation time. (F) The A_{650}/A_{530} of E_2apt and Fe_3O_4@Au system at different incubation time. (G) The A_{650}/A_{530} of the system under different NaCl concentration with the reaction time of 5 and 25 min. The error bars represent the standard deviation ($n = 3$), values in figures with the same superscript letter are not significantly different.

905.39 ms and 1117.73 ms. These phenomena were caused by competition between Fe_3O_4@Au and E_2. When the target analyte E_2 was presented in the system, the aptamer would fall off the surface of NPs and specifically bound to E_2. Meanwhile, NaCl would induce the aggregation and sedimentation of NPs, which caused the reduction of evenly dispersed NPs. Hence, the effect of inhomogeneities on surrounding water proton reduced and the T_{2w} increased relatively. And the higher the target concentration, the smaller the impact of inhomogeneities, thus the larger the variation range of T_{2w}.

The relationship between the concentration of the detection system and ΔT_{2w} is shown in Fig. 2(B). When the Fe_3O_4@Au@Apt concentration was fixed, ΔT_{2w} showed an upward trend with the increase of E_2 concentration. And the ΔT_{2w} of the system would also change with the concentration of Fe_3O_4@Au@Apt when E_2 concentration was constant. The results revealed that the highest

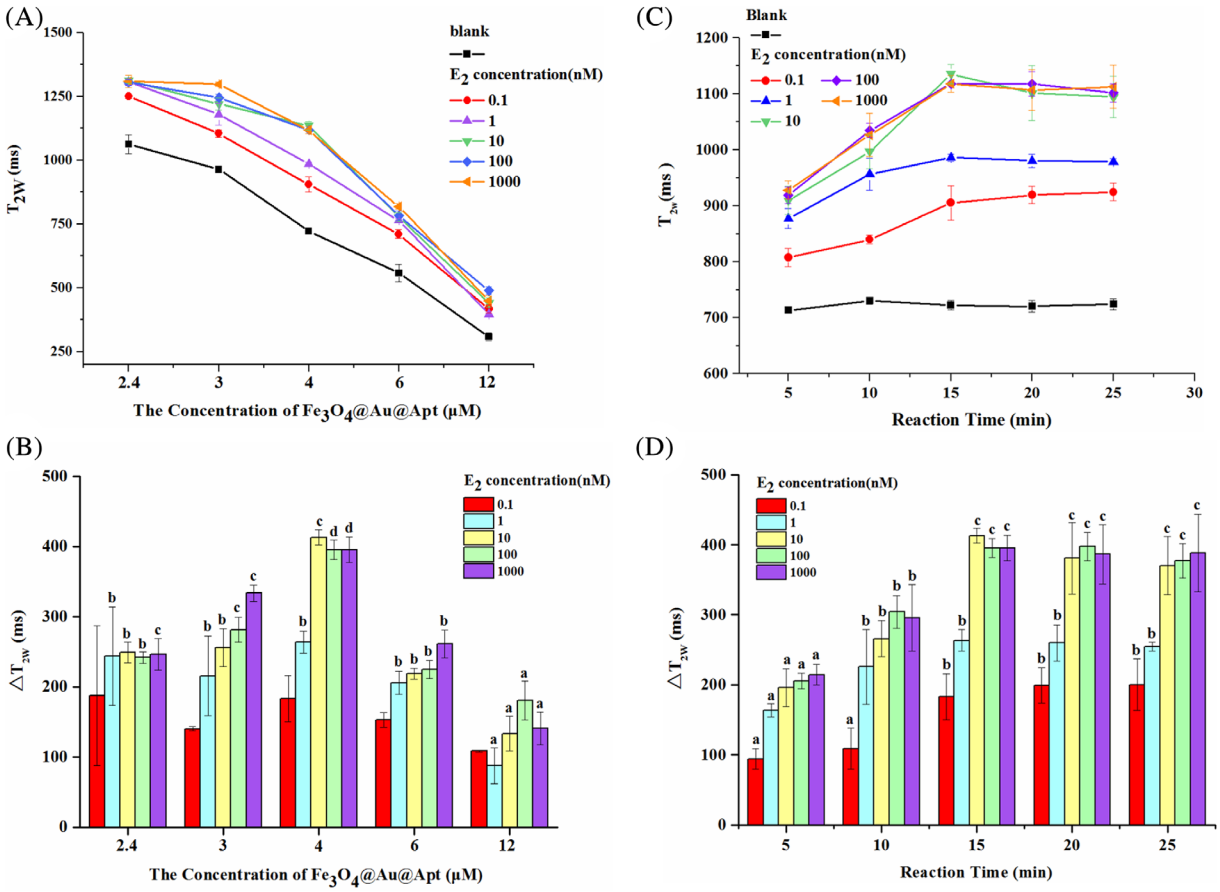

Figure 2. Condition optimization of the MRS sensor. (A,B) Effect of concentration of Fe_3O_4@Au@Apt and E_2 on T_{2w} and ΔT_{2w}. (C,D) Effect of reaction time of Fe_3O_4@Au@Apt and E_2 on T_{2w} and ΔT_{2w}. The error bars represent the standard deviation ($n = 3$), values in figures with the same superscript letter are not significantly different.

ΔT_{2w} value was detected when the concentration of Fe_3O_4@Au@Apt was 4 μmol L^{-1}. And ΔT_{2w} value at this point was significantly higher than that of other groups at E_2 concentration of 10 to 1000 nmol L^{-1}. Meanwhile, as reported by Chen *et al.*,[34] who employed the functionalized-superparamagnetic iron oxide NPs as MRS sensor to monitor kanamycin, the concentration of NPs should be chosen as the optimal concentration when the maximum ΔT_2 value was reached, and this would be helpful for the improvement of detection sensitivity. Thus, to ensure optimal performance, the concentration of Fe_3O_4@Au@Apt was selected to be 4 μmol L^{-1} in this study.

The reaction time of Fe_3O_4@Au@Apt and E_2

The reaction time of Fe_3O_4@Au@Apt and E_2 was optimized to enhance the sensitivity of detection. As shown in Fig. 2(C), the T_{2w} of the blank groups were between 713.29 and 730.63 ms, which were almost unaffected by the reaction time. However, the T_{2w} of the experimental groups relatively increased with the extension of reaction time. For example, the T_{2w} of the system with 0.1 nmol L^{-1} E_2 increased from 807.56 to 905.39 ms when the reaction time was extended from 5 to 15 min. After a reaction time of 15 min, the magnetic response signal became relatively stable, and the T_{2w} increased from 905.39 to 1117.73 ms when the E_2 concentration increased from 0.1 to 1000 nmol L^{-1}, showing that Fe_3O_4@Au@Apt and E_2 had fully reacted within 15 min.

The reaction time also has significant impacts on ΔT_{2w}.[31] As shown in Fig. 2(D), the value of ΔT_{2w} for each group was relatively small when reacting for only 5 min. The ΔT_{2w} was only 94.27 ms at E_2 concentration of 0.1 nmol L^{-1}. A possible explanation for this might be that Fe_3O_4@Au@Apt and E_2 had not fully reacted, thus there were only minor changes in the magnetic relaxation signal. With the extension of reaction time, the reactions between Fe_3O_4@Au@Apt and E_2 tended to be sufficient, and the influence on the magnetic response of the system would be enhanced, which was manifested as the relative increase of system ΔT_{2w}. After reacting for 15 min, the ΔT_{2w} of the system with different E_2 concentrations tended to be stable, for example, the ΔT_{2w} of the system with 0.1 nmol L^{-1} E_2 significantly increased to 183.04 ms. Therefore, 15 min was selected as the optimal reaction time for Fe_3O_4@Au@Apt and E_2.

Sensitivity of the MRS sensor and the standard curve

The sensitivity of the detection method was evaluated based on the optimization of the reaction conditions. As shown in Fig. 3 (A), the ΔT_{2w} increased from 190 to 410.66 ms with an increase in E_2 concentration. A good linear correlation was found when E_2 concentration was between 0.1 and 10 nmol L^{-1} and the standard curve was as follows:

$$Y = 20.269x + 210.818, R^2 = 0.960$$

This indicates that the E_2 concentration in the system can be quantified through ΔT_{2w} value. According to a signal-to-noise ratio (*S/N*) of 3, the LOD of the MRS sensor for E_2 detection was

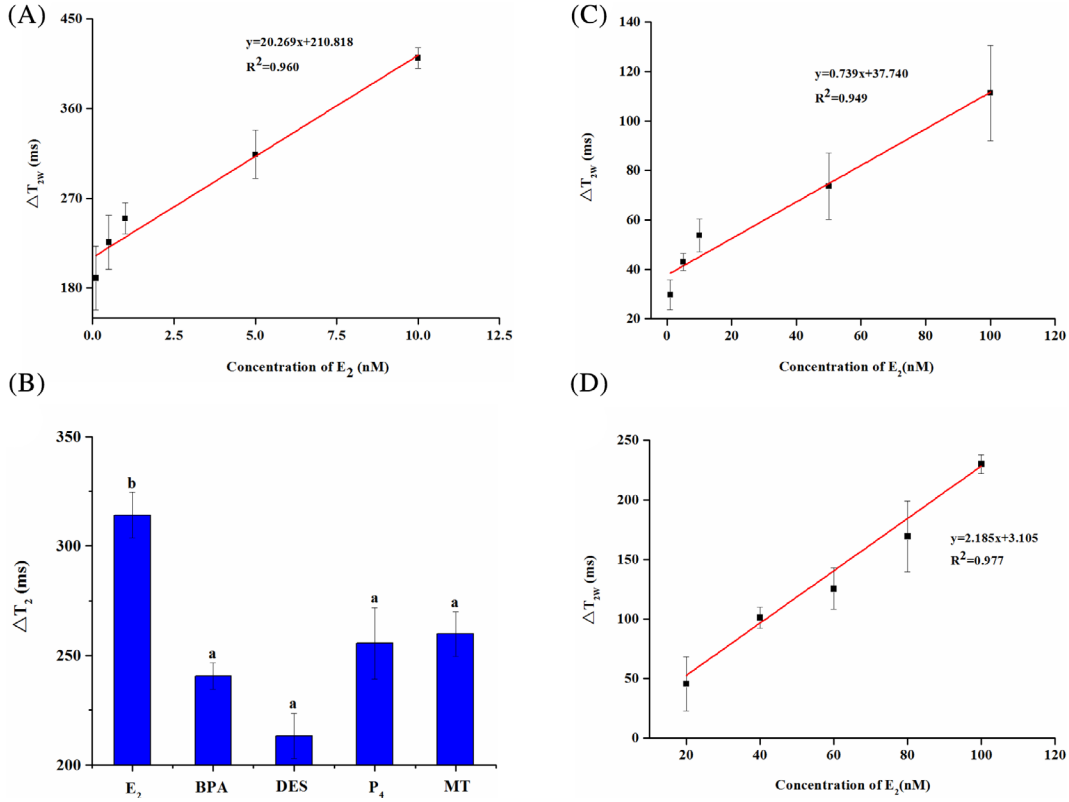

Figure 3. Investigation of the sensitivity, selectivity and feasibility of the MRS sensor for E_2 detection. (A) Linear relationship between the ΔT_{2w} value and the concentration of E_2. (B) The selectivity of MRS sensor. (C) Calibration curve of MRS sensor for E_2 in milk sample. (D) Calibration curve of MRS sensor for E_2 in eggs sample. The error bars represent the standard deviation ($n = 5$), values in figures with the same superscript letter are not significantly different.

calculated to be 0.843 nmol L^{-1}. The comparison of linear range and LOD between the developed MRS sensor and other published E_2 detection methods is presented in Table 1. When detecting estradiol in water systems, the LOD of the designed sensor was better than those of Lu and Xu,[10] Zhang *et al.*,[17] Yildirim *et al.*[21] and Fang *et al.*[61] Although the method designed by Nameghi's

Table 1. Comparison of parameters of other published sensors used for 17β-estradiol (E_2) detection

Detection method	Aptamer length (mer)	Linear range (nmol L^{-1})	Limit of detection (nmol L^{-1})	Sample	Recovery (%)	Relative standard deviation (%)	References
HPLC		1.84–367	1.47	Tap water	87.0–94.0	4.0–5.0	10
				Lake water	87.0–93.0	4.0	
				River water	86.0–92.0	4.0–5.0	
Colorimetry	76	—	0.2	Saliva	—	—	38
Colorimetry	76	1.57–350	1.57	Water	104.5–114.5	2.79–4.34	17
SERS		—	300	River water	—	—	61
Fluorescence	76	—	2.1	Wastewater	95–105	1.3–3.9	21
Fluorescence		0.35–3.5 × 10^4	0.35	Tap water	96.2–106.9	3.9–5.4	20
				Environmental water	96.3–104.0	2.8–3.8	
				Urine	91.4–110.8	5.4–9.0	
				Milk	92.4–120.6	10.3–14.3	
Fluorescence	35	80–400	37	Fetal bovine serum (FBS)	96.5–104.8	2.2–10.1	19
Electrochemical	76	5 × 10^{-4} -5	6.0 × 10^{-5}	Urine	96.3–104.3	1.4–3.5	22
Electrochemical		1.2 × 10^{-3} –0.1 and 0.1–7	5 × 10^{-4}	Tap water			62
Magnetic	76	0.1–10	0.843	Deionized water	—	—	This work
relaxation		1–100	7.6	Milk	101.93–120.8	5.43–14.57	
switching		20–100	8.57	Eggs	94.18–100.98	3.39–9.99	

Table 2. Recoveries of 17β-estradiol (E_2) in milk and eggs samples

Sample	E_2 added (nmol L^{-1})	E_2 found (nmol L^{-1})	Recovery (%, $n = 5$)	Relative standard deviation (%, $n = 5$)
Milk	10	12.08	120.80	14.57
	50	52.98	105.96	5.43
	100	101.93	101.93	10.10
Eggs	20	18.90	94.50	7.49
	60	56.51	94.18	9.99
	100	100.98	100.98	3.39

group[62] showed a much better LOD (5×10^{-4} nmol L^{-1}), the fabrication of their sensor required the immobilization of aptamer and modification of electrodes, which was more complicated. Compared with other E_2 detection methods based on 76 mer nucleic acid aptamer, the LOD of this method was equivalent to that of Soh *et al.*[38] and Zhang *et al.*,[17] indicating that the aptamer has good E_2 recognition ability. In summary, this MRS sensor was capable of detecting the E_2 pollution.

Specificity of the MRS sensor

To better illustrate the potential application of this method, the specificity of the designed MRS sensor was evaluated. The E_2 and four interferons in the linear detection concentration range (5 nmol L^{-1}) were tested. As shown in Fig. 3(B), the ΔT_{2w} of the E_2 system (314.06 ms) was significantly higher than that of the DES system (217.77 ms) and BPA system (205.20 ms). Although the ΔT_{2w} of the MT system (259.80 ms) and P_4 system (255.52 ms) were relatively larger, they were still clearly distinguished from the E_2 system. These results suggest that the proposed MRS sensor has specificity for E_2 detection in a complex matrix.

Detection of E_2 in spiked samples

To evaluate the accuracy and potential application of the developed MRS sensor, the method was applied to two kinds of food samples, milk, and eggs. As shown in Fig. 3(C), there was a good linear relationship between ΔT_{2w} and E_2 concentration when E_2 concentration in milk samples was 1–100 nmol L^{-1}. The LOD was determined to be 7.6 nmol L^{-1} ($S/N = 3$). And the standard curve was as follows:

$$y = 0.739x + 37.740, R^2 = 0.949$$

As shown in Fig. 3(D), the E_2 can be quantified over a concentration range of 20 to 100 nmol L^{-1} with a detection limit of 8.57 nmol L^{-1} for spiked egg samples. And the standard curve was as follows:

$$y = 2.185x + 3.105, R^2 = 0.977$$

It was worth noting that the spiked food samples all showed higher LOD and wider linear ranges than that of the water system. A possible explanation for this might be that the milk and egg samples contained methionine, and methionine could absorb on the surface of Au NPs by forming Au–S and Au–N bonds, thus suppressing the salt-induced aggregation of NPs,[63] accordingly reducing the change of ΔT_{2w} and showing a higher LOD.

The accuracy of the MRS sensor was performed by examining the recoveries of spiked samples. The precision of the MRS sensor was evaluated by calculating the RSD of the samples at different concentration levels. The recovery results of E_2 in the two different samples are shown in Table 2, the recoveries of spiked milk and egg samples detected by the MRS sensor were achieved in the ranges 101.93–120.8% and 94.18–100.98%, respectively. The RSDs of spiked milk and egg samples were less than 14.57% and 9.99%, respectively. As shown in Table 2, when detecting E_2 in milk, the recovery value of the MRS sensor was better than that of fluorescence,[20] and its RSD was lower. When detecting E_2 in eggs, the developed MRS sensor provided good recovery values and RSD values. These results suggested that the MRS sensor has a great potential for E_2 detection in food sample.

CONCLUSIONS

In conclusion, we successfully designed new aptamers modified Fe_3O_4@Au NPs as the MRS sensor for sensitive and selective detection of E_2 in milk and eggs. In the presence of E_2, the aptamer would bind with E_2 and separate from the surface of Fe_3O_4@Au, thereby destroying the homogenous magnetic filed for water protons, resulting in an increase in the T_2 value of the detection system. According to the sensing effect of the present MRS sensor for E_2, the volume ratio of aptamers and Fe_3O_4@Au, the concentration of NaCl, the concentration of Fe_3O_4@Au@Apt and reaction time were optimized. The sensor showed a wide linear range from 0.1 to 10 nmol L^{-1} and a low detection limit of 0.843 nmol L^{-1}. Moreover, the developed sensor was successfully used for E_2 determination among food samples. In the detection of E_2 in milk and egg samples, the linear ranges of the sensor were 1–100 nmol L^{-1} and 20–100 nmol L^{-1}, and the LODs were 7.4 and 8.57 nmol L^{-1}, respectively. In general, the MRS sensor designed in this study exhibits a simple, rapid and efficient way for detecting E_2, which has potential applications in the livestock and poultry food system.

ACKNOWLEDGEMENTS

This work was supported by the National Natural Science Foundation of China (NSFC China 81773482).

SUPPORTING INFORMATION

Supporting information may be found in the online version of this article.

REFERENCES

1 Dong X, He L, Hu H, Liu N, Gao S and Piao Y, Removal of 17β-estradiol by using highly adsorptive magnetic biochar nanoparticles from aqueous solution. *Chem Eng J* **352**:371–379 (2018).
2 Russo R, Cavaliere F, Watanabe C, Nucci C, Bagetta G, Corasaniti MT *et al.*, 17β-Estradiol prevents retinal ganglion cell loss induced by

acute rise of intraocular pressure in rat, in *Glaucoma: An Open Window to Neurodegeneration and Neuroprotection*, Progress in Brain Research, Netherlands, pp. 583–590 (2008).
3 Chang HS, Choo KH, Lee B and Choi SJ, The methods of identification, analysis, and removal of endocrine disrupting compounds (EDCs) in water. *J Hazard Mater* **172**:1–12 (2009).
4 Nezami A, Nosrati R, Golichenari B, Rezaee R, Chatzidakis GI, Tsatsakis AM *et al*., Nanomaterial-based aptasensors and bioaffinity sensors for quantitative detection of 17β-estradiol. *TrAC Trends Anal Chem* **94**:95–105 (2017).
5 Xiong X, Li D, Du Z, Xiong C and Jiang H, Magnetic solid-phase extraction modified Quick, Easy, Cheap, Effective, Rugged and Safe method combined with pre-column derivatization and ultra-high performance liquid chromatography-tandem mass spectrometry for determination of estrogens and estrogen mimics in pork and chicken samples. *J Chromatogr A* **1622**:461137 (2020).
6 Lu H and Xu S, Hollow mesoporous structured molecularly imprinted polymers for highly sensitive and selective detection of estrogens from food samples. *J Chromatogr A* **1501**:10–17 (2017).
7 Courant F, Antignac JP, Laille J, Monteau F, Andre F and le Bizec B, Exposure assessment of prepubertal children to steroid endocrine disruptors. 2. Determination of steroid hormones in milk, egg, and meat samples. *J Agric Food Chem* **56**:3176–3184 (2008).
8 Tang J, Wang J, Yuan L, Xiao Y, Wang X and Yang Z, Trace analysis of estrogens in milk samples by molecularly imprinted solid phase extraction with genistein as a dummy template molecule and high-performance liquid chromatography–tandem mass spectrometry. *Steroids* **145**:23–31 (2019).
9 Socas-Rodriguez B, Asensio-Ramos M, Hernandez-Borges J and Rodriguez-Delgado MA, Analysis of oestrogenic compounds in dairy products by hollow-fibre liquid-phase microextraction coupled to liquid chromatography. *Food Chem* **149**:319–325 (2014).
10 Lu H and Xu S, Mesoporous structured estrone imprinted Fe3O4@SiO2@mSiO2 for highly sensitive and selective detection of estrogens from water samples by HPLC. *Talanta* **144**:303–311 (2015).
11 Wang J, Cheng C and Yang Y, Determination of estrogens in milk samples by magnetic-solid-phase extraction technique coupled with high-performance liquid chromatography. *J Food Sci* **80**:C2655–C2661 (2015).
12 Fedeniuk RW, Boison JO and MacNeil JD, Validation of a gas chromatography-mass spectrometry method for the determination of pg/ml levels of 17beta-estradiol and 17beta-trenbolone in bovine serum. *J Chromatogr B Analyt Technol Biomed Life Sci* **802**:307–315 (2004).
13 Kawaguchi M, Ito R, Sakui N, Okanouchi N, Saito K and Nakazawa H, Dual derivatization-stir bar sorptive extraction-thermal desorption-gas chromatography-mass spectrometry for determination of 17beta-estradiol in water sample. *J Chromatogr A* **1105**:140–147 (2006).
14 Stopforth A, Burger BV, Crouch AM and Sandra P, The analysis of estrone and 17beta-estradiol by stir bar sorptive extraction-thermal desorption-gas chromatography/mass spectrometry: application to urine samples after oral administration of conjugated equine estrogens. *J Chromatogr B Analyt Technol Biomed Life Sci* **856**:156–164 (2007).
15 Gao Q, Luo D, Bai M, Chen ZW and Feng YQ, Rapid determination of estrogens in milk samples based on magnetite nanoparticles/polypyrrole magnetic solid-phase extraction coupled with liquid chromatography-tandem mass spectrometry. *J Agric Food Chem* **59**:8543–8549 (2011).
16 Yan W, Li Y, Zhao L and Lin JM, Determination of estrogens and bisphenol A in bovine milk by automated on-line C30 solid-phase extraction coupled with high-performance liquid chromatography-mass spectrometry. *J Chromatogr A* **1216**:7539–7545 (2009).
17 Zhang D, Zhang W, Ye J, Zhan S, Xia B, Lv J *et al*., A label-free colorimetric biosensor for 17β-Estradiol detection using nanoparticles assembled by aptamer and cationic polymer. *Austr J Chem* **69**:12–19 (2016).
18 Fan L, Zhao G, Shi H and Liu M, A simple and label-free aptasensor based on nickel hexacyanoferrate nanoparticles as signal probe for highly sensitive detection of 17beta-estradiol. *Biosens Bioelectron* **68**:303–309 (2015).
19 Huang H, Shi S, Gao X, Gao R, Zhu Y, Wu X *et al*., A universal label-free fluorescent aptasensor based on Ru complex and quantum dots for adenosine, dopamine and 17beta-estradiol detection. *Biosens Bioelectron* **79**:198–204 (2016).
20 Zhang G, Li T, Zhang J and Chen A, A simple FRET-based turn-on fluorescent aptasensor for 17β-estradiol determination in environmental water, urine and milk samples. *Sens Actuators B* **273**:1648–1653 (2018).
21 Yildirim N, Long F, Gao C, He M, Shi HC and Gu AZ, Aptamer-based optical biosensor for rapid and sensitive detection of 17beta-estradiol in water samples. *Environ Sci Technol* **46**:3288–3294 (2012).
22 Huang K-J, Liu Y-J and Zhang J-Z, Aptamer-based electrochemical assay of 17β-estradiol using a glassy carbon electrode modified with copper sulfide nanosheets and gold nanoparticles, and applying enzyme-based signal amplification. *Microchim Acta* **182**:409–417 (2014).
23 Gu G-Y, Wang X, Zhou H-L and Liu B-L, Progresses of magnetic relaxation switch sensor in medical diagnosis and food safety analysis. *Chin J Anal Chem* **46**:1161–1170 (2018).
24 Liu Y, Cai Z, Sheng L, Ma M and Wang X, A magnetic relaxation switching and visual dual-mode sensor for selective detection of Hg(2+) based on aptamers modified Au@Fe3O4 nanoparticles. *J Hazard Mater* **388**:121728 (2020).
25 Zhang Y, Shen J, Yang H, Yang Y, Zhou Z and Yang S, A highly selective magnetic sensor for Cd2+ in living cells with (Zn, Mn)-doped iron oxide nanoparticles. *Sens Actuators B* **207**:887–892 (2015).
26 Zhang Y, Zhao Y, Yang Y, Shen J, Yang H, Zhou Z *et al*., A bifunctional sensor based on Au-Fe3O4 nanoparticle for the detection of Cd2+. *Sens Actuators B* **220**:622–626 (2015).
27 Cai S, Liang G, Zhang P, Chen H, Zhang S, Liu B *et al*., A miniature chip for protein detection based on magnetic relaxation switches. *Biosens Bioelectron* **26**:2258–2263 (2011).
28 Silva RN, Vijayan AN, Westbrook E, Yu Z and Zhang P, Nanoparticle assisted nuclear relaxation-based oligonucleotide detection. *Anal Chim Acta* **1062**:118–123 (2019).
29 Liang G, Cai S, Zhang P, Peng Y, Chen H, Zhang S *et al*., Magnetic relaxation switch and colorimetric detection of thrombin using aptamer-functionalized gold-coated iron oxide nanoparticles. *Anal Chim Acta* **689**:243–249 (2011).
30 Zou D, Jin L, Wu B, Hu L, Chen X, Huang G *et al*., Rapid detection of Salmonella in milk by biofunctionalised magnetic nanoparticle cluster sensor based on nuclear magnetic resonance. *Int Dairy J* **91**:82–88 (2019).
31 Zhao Y, Li Y, Jiang K, Wang J, White WL, Yang S *et al*., Rapid detection of *Listeria monocytogenes* in food by biofunctionalized magnetic nanoparticle based on nuclear magnetic resonance. *Food Control* **71**:110–116 (2017).
32 Perez JM, Simeone FJ, Saeki Y, Josephson L and Weissleder R, Viral-induced self-assembly of magnetic nanoparticles allows the detection of viral particles in biological media. *J Am Chem Soc* **125**:10192–10193 (2003).
33 Shen J, Yang Y, Zhang Y, Yang H, Zhou Z and Yang S, Functionalized Au-Fe3O4 nanocomposites as a magnetic and colorimetric bimodal sensor for melamine. *Sens Actuators B* **226**:512–517 (2016).
34 Chen YP, Zou M q, Qi C, Xie M-X, Wang D-N, Wang Y-F *et al*., Immunosensor based on magnetic relaxation switch and biotin–streptavidin system for the detection of kanamycin in milk. *Biosens Bioelectron* **39**:112–117 (2013).
35 Xu Z-C, Hou Y-L and Sun S-H, Magnetic Core/Shell Fe3O4/Au and Fe3O4/Au/Ag nanoparticles with tunable plasmonic properties. *J Am Chem Soc* **129**:8698–8699 (2007).
36 Karami C and Taher MA, A catechol biosensor based on immobilizing laccase to Fe3O4@Au core-shell nanoparticles. *Int J Biol Macromol* **129**:84–90 (2019).
37 Kim YS, Jung HS, Matsuura T, Lee HY, Kawai T and Gu MB, Electrochemical detection of 17beta-estradiol using DNA aptamer immobilized gold electrode chip. *Biosens Bioelectron* **22**:2525–2531 (2007).
38 Soh JH, Lin Y, Rana S, Ying JY and Stevens MM, Colorimetric detection of small molecules in complex matrixes via target-mediated growth of aptamer-functionalized gold nanoparticles. *Anal Chem* **87**:7644–7652 (2015).
39 Fan L, Zhao G, Shi H, Liu M, Wang Y and Ke H, A femtomolar level and highly selective 17beta-estradiol photoelectrochemical aptasensor applied in environmental water samples analysis. *Environ Sci Technol* **48**:5754–5761 (2014).
40 Atashi Z, Divband B, Keshtkar A, Khatamian M, Farahmand-Zahed F, Nazarlo AK *et al*., Synthesis of cytocompatible Fe3O4@ZSM-5 nanocomposite as magnetic resonance imaging contrast agent. *J Magn Magn Mater* **438**:46–51 (2017).

41 Meiboom S and Gill D, Modified spin-echo method for measuring nuclear relaxation times. *Rev Sci Instrum* **29**:688–691 (1958).
42 Li L, Li B, Cheng D and Mao L, Visual detection of melamine in raw milk using gold nanoparticles as colorimetric probe. *Food Chem* **122**: 895–900 (2010).
43 Ma Q, Wang Y, Jia J and Xiang Y, Colorimetric aptasensors for determination of tobramycin in milk and chicken eggs based on DNA and gold nanoparticles. *Food Chem* **249**:98–103 (2018).
44 Karamipour S, Sadjadi MS and Farhadyar N, Fabrication and spectroscopic studies of folic acid-conjugated Fe3O4@Au core-shell for targeted drug delivery application. *Spectrochim Acta A* **148**:146–155 (2015).
45 Banerjee S, Raja SO, Sardar M, Gayathri N, Ghosh B and Dasgupta A, Iron oxide nanoparticles coated with gold: enhanced magnetic moment due to interfacial effects. *J Appl Phys* **109**:123902 (2011).
46 Pabisch S, Feichtenschlager B, Kickelbick G and Peterlik H, Effect of interparticle interactions on size determination of zirconia and silica based systems – a comparison of SAXS, DLS, BET, XRD and TEM. *Chem Phys Lett* **521**:91–97 (2012).
47 Banerjee S, Kumar NP, Srinivas A and Roy S, Core-shell Fe3O4@Au nanocomposite as dual-functional optical probe and potential removal system for arsenic (III) from water. *J Hazard Mater* **375**:216–223 (2019).
48 Sood A, Arora V, Shah J, Kotnala RK and Jain TK, Multifunctional gold coated iron oxide core-shell nanoparticles stabilized using thiolated sodium alginate for biomedical applications. *Mater Sci Eng C-Mater* **80**:274–281 (2017).
49 Min C, Shao HL, Liong M, Yoon TJ, Weissleder R and Lee H, Mechanism of magnetic relaxation switching sensing. *ACS Nano* **6**:6821–6828 (2012).
50 Lin SC, Gan N, Cao YT, Chen YJ and Jiang QL, Selective dispersive solid phase extraction-chromatography tandem mass spectrometry based on aptamer-functionalized UiO-66-NH2 for determination of polychlorinated biphenyls. *J Chromatogr A* **1446**:34–40 (2016).
51 Kim YS, Kim JH, Kim IA, Lee SJ, Jurng J and Gu MB, A novel colorimetric aptasensor using gold nanoparticle for a highly sensitive and specific detection of oxytetracycline. *Biosens Bioelectron* **26**:1644–1649 (2010).
52 Liu CW, Hsieh YT, Huang CC, Lin ZH and Chang HT, Detection of mercury(II) based on Hg2+ -DNA complexes inducing the aggregation of gold nanoparticles. *Chem Commun (Camb)* **19**: 2242–2244 (2008).
53 Shen Q, Nie Z, Guo M, Zhong CJ, Lin B, Li W *et al.*, Simple and rapid colorimetric sensing of enzymatic cleavage and oxidative damage of single-stranded DNA with unmodified gold nanoparticles as indicator. *Chem Commun (Camb)* **8**:929–931 (2009).
54 Niazi JH, Lee SJ, Kim YS and Gu MB, ssDNA aptamers that selectively bind oxytetracycline. *Bioorg Med Chem* **16**:1254–1261 (2008).
55 Apyari VV, Dmitrienko SG, Arkhipova VV, Atnagulov AG, Gorbunova MV and Zolotov YA, Label-free gold nanoparticles for the determination of neomycin. *Spectrochim Acta A* **115**:416–420 (2013).
56 Li X, Cheng R, Shi H, Tang B, Xiao H and Zhao G, A simple highly sensitive and selective aptamer-based colorimetric sensor for environmental toxins microcystin-LR in water samples. *J Hazard Mater* **304**:474–480 (2016).
57 Kaittanis C, Naser SA and Perez JM, One-step, nanoparticle-mediated bacterial detection with magnetic relaxation. *Nano Lett* **7**:380–383 (2007).
58 Kurlyandskaya G and Levit V, Magnetic Dynabeads (R) detection by sensitive element based on giant magnetoimpedance. *Biosens Bioelectron* **20**:1611–1616 (2005).
59 Baselt DR, Lee GU, Natesan M, Metzger SW, Sheehan PE and Colton RJ, A biosensor based on magnetoresistance technology. *Biosens Bioelectron* **13**:731–739 (1998).
60 Wang W, Ma P, Dong H, Krause HJ, Zhang Y, Willbold D *et al.*, A magnetic nanoparticles relaxation sensor for protein-protein interaction detection at ultra-low magnetic field. *Biosens Bioelectron* **80**:661–665 (2016).
61 Fang C, Bandaru NM, Ellis AV and Voelcker NH, Beta-cyclodextrin decorated nanostructured SERS substrates facilitate selective detection of endocrine disruptorchemicals. *Biosens Bioelectron* **42**:632–639 (2013).
62 Nameghi MA, Danesh NM, Ramezani M, Alibolandi M, Abnous K and Taghdisi SM, An ultrasensitive electrochemical sensor for 17beta-estradiol using split aptamers. *Anal Chim Acta* **1065**:107–112 (2019).
63 Huang P-C, Gao N, Li J-F and Wu F-Y, Colorimetric detection of methionine based on anti-aggregation of gold nanoparticles in the presence of melamine. *Sens Actuators B* **255**:2779–2784 (2018).